J Physiol Sci (2009) 59:227–241
DOI 10.1007/s12576-009-0032-z

ORIGINAL PAPER

Inhomogeneous distribution of action potential characteristics in the rabbit sino-atrial node revealed by voltage imaging

Haruko Masumiya · Yoshitaka Oku · Yasumasa Okada

Received: 7 August 2008 / Accepted: 3 February 2009 / Published online: 19 March 2009

Abstract The sino-atrial node (SAN) is the natural pacemaker of the heart. Mechanisms of the leading pacemaker site generation and dynamic pacemaker shifts in the SAN have been so far studied with an electrophysiological technique, but the detailed spatial distribution of action potential characteristics in the SAN has not been analyzed due to the limited number of simultaneously recorded sites in microelectrode recording. To elucidate the mechanism of leading pacemaker site generation in the SAN, we applied a voltage imaging technique and analyzed the spatial distribution of action potential characteristics in the rabbit SAN. Action potential parameters, i.e., action potential duration at 50% repolarization level, the slope of upstroke, and the slope of the linearly depolarizing early phase of pacemaker activity (phase-4), were calculated from optical signals. Action potential parameter values derived from intracellular recording with a microelectrode and those from optical recording were significantly correlated. The leading pacemaker site occurred in the region of either globally or locally maximum phase-4 slope in 7 of 12 preparations, however, it did not coincide with the region of the early maximum phase-4 slope in the other 5 preparations. Carbenoxolone, a gap junction blocker, changed action potential properties and caused pacemaker shifts. Model simulation, assuming an inhomogeneous distribution of intrinsic properties of SAN cells, reproduced the experimental results. We conclude that the functional structure of the SAN is more inhomogeneous than that dictated by previous models. Besides intrinsic cellular properties, cell-to-cell interaction through gap junctions influences action potential characteristics and leading pacemaker site generation.

Keywords Optical imaging · Voltage-sensitive dye · Gap junction · Pacemaker shift · Simulation

H. Masumiya · Y. Oku (✉)
Division of Physiome, Department of Physiology,
Hyogo College of Medicine, Nishinomiya,
Hyogo 663-8501, Japan
e-mail: yoku@hyo-med.ac.jp

Y. Okada
Department of Medicine, Keio University Tsukigase
Rehabilitation Center, Izu, Shizuoka 410-3215, Japan

Introduction

The pacemaking mechanism in the sino-atrial node (SAN) has been extensively studied morphologically and electrophysiologically [1–3]. Electrophysiological properties of SAN cells studied by microelectrode recording have indicated a gradual transition from the center to the periphery, and two models have been proposed to account for this gradual transition [4]. The mosaic model hypothesizes a gradual increase in the ratio of atrial cells to SAN cells from the center to the periphery [5]. The gradient model assumes a gradual change in intrinsic properties of SAN cells from the center to the periphery [1, 6], in which the leading pacemaker site occurs in the region of maximum action potential duration and maximum phase-4 slope. These two models have a common feature in the sense that they a priori endow the central region with intrinsic properties of the leading pacemaker. However, morphological studies [7, 8] have emphasized that nerves, ganglia, and small myocytes constitute a complex anatomical structure of the SAN. Therefore, we hypothesized that the pacemaker organization is functionally and anatomically more complex than the previously assumed gradient or mosaic configuration. Jalife [9] has postulated that the leading pacemaker site emerges as a consequence of mutual entrainment of SAN cells. This

concept, presented in 1984, can still be assumed as the underlying mechanism of pacemaker synchronization in the compact region of the SAN in either the gradient or mosaic model. According to this concept, we further hypothesized that, provided that the SAN structure is more complex, changes in gap junction conductance should greatly influence the action potential characteristics and could induce abrupt pacemaker shifts. In the present study, we visualized excitation propagation within the rabbit SAN in vitro by optical recording using a voltage-sensitive dye and tested these hypotheses.

An advantage of an optical imaging technique is the ability to simultaneously analyze multipoint activities in the region of interest including the whole SAN region. Its spatial resolution is sufficiently high to characterize the dynamically changing leading pacemaker site [10]. In contrast, the number of simultaneously recorded sites in extracellular mapping systems is often insufficient to detect dynamic pacemaker shifts [11]. One limitation of optical mapping of the heart is motion artifacts introduced by muscle contraction [12]. Muscle contraction can be suppressed by using electromechanical uncoupling agents. However, these agents themselves distort action potential shapes and thus we avoided the usage of electromechanical uncoupling agents as others described previously [13]. Since the artifact caused by muscle contraction primarily can distort optical signals during the repolarization phase [12], characterization of action potentials during the depolarization phase is not influenced by motion artifacts and thus is feasible for evaluation. Therefore, in the present study, we attempted to estimate action potential characteristics mainly during the depolarization phase and evaluated their changes after the reduction of gap junction conductance. Further, we made a model simulation to test whether the behavior of the hypothesized SAN structure agrees with the experimental results.

Methods

Animal preparation

All experiments were conducted in accordance with the Guiding Principles for the Care and Use of Animals in the Field of Physiological Sciences [14]. Also, the experimental protocols were approved by the Animal Research Committee at Hyogo College of Medicine.

Japanese white rabbits ($n = 14$; 2.4–2.8 kg) of both sexes purchased from Japan SLC (Hamamatsu, Japan) were anesthetized by intravenous injection of sodium pentobarbital (30 mg/kg), and the heart was quickly isolated. The SAN preparation was made as we described previously [15–17]. Briefly, the right atrial tissue containing the anterior wall, superior vena cava (SVC), inferior vena cava (IVC), and the auricle were isolated en bloc. Then, the SVC was opened by cutting the free wall side of the SVC so that the right atrium side of the SVC tissue was not damaged. The SAN region extends from the crista terminalis (CT) towards the opening of the SVC [18]. Thus the tissues including the SAN region, approximately 5 × 5 mm in size, were cut out perpendicularly to the CT. Preparations were incubated with a voltage-sensitive dye, di-4-ANEPPS (20 μM; Invitrogen, Carlsbad, CA, USA) for 20 min in an oxygenated (95% O_2 and 5% CO_2) physiological solution with the following composition (in mM): NaCl 118.4, KCl 4.7, $CaCl_2$ 2.5, $MgSO_4$ 1.2, KH_2PO_4 1.2, $NaHCO_3$ 24.9, and glucose 11.1 (pH 7.4) [15, 16]. After staining, preparations were pinned down horizontally with the endocardial side up on a silicon floor in a recording chamber (volume 2.5 ml) filled with the physiological solution and were perfused at a rate of 1.5–2.0 ml/min. The temperature of the organ bath was maintained at 34.0°C. In some cases ($n = 6$), a selective gap junction blocker carbenoxolone (100 μM) was applied at least 20 min, and its effect was evaluated.

ECG recording

Electrical field potential of the SAN was recorded with a pair of fine metal electrodes placed on both edges of the preparation. Signals were amplified with a bioelectric amplifier (AB-611J, Nihon Kohden, Tokyo, Japan) and fed into a time-amplitude window discriminator (EN611J, Nihon Kohden, Tokyo, Japan). The window discriminator generated a TTL-level pulse signal when the field potential exceeded the minimum preset threshold level, and the TTL pulse was used to trigger the optical recording system at the onset of pacemaker activity [19, 20].

Voltage imaging

The recording chamber was mounted on a fluorescence macro zoom microscope (MVX-10, Olympus Optical, Tokyo, Japan), and the preparation was illuminated with a tungsten-halogen lamp (150 W) through a band-pass excitation filter ($\lambda = 480$–550 nm). To reduce dye-induced photodynamic damage to cardiomyocytes, we minimized the exposure time of excitation light using a computer-controlled electric shutter. Also, we adjusted the intensity of excitation light using a neutral density filter based on our preliminary study so that the electrocardiogram did not substantially change with exposure to excitation light. Fluorescence through a long-pass emission filter (>590 nm) was detected by a CMOS sensor array (MiCAM Ultima L-camera, Brainvision, Tokyo, Japan) with a 100 × 100 μm pixel size (100 × 100 pixels array) at time resolutions of 0.5,

1.0, or 2.0 ms/frame as we described previously [19–21]. A total of 256, 512, or 1,024 frames were recorded starting at 192, 384, or 768 frames before the onset of pacemaker activity (75% post-trigger mode) and averaged 5–13 times. Magnification of the microscope was adjusted to 1.25–3.3× depending on the region of interest. One pixel corresponded to 80 × 80–30 × 30 μm, and the image sensor covered a total of 8 × 8–3 × 3 mm^2.

Analysis of imaging data

The change in fluorescence intensity (ΔF) relative to the initial intensity of the fluorescence (F_0) in each pixel was calculated. To normalize the difference in the amount of membrane-bound dye and illumination within the preparation, background fluorescence intensity at each pixel was divided by the maximum background fluorescence, and then the ratio of ΔF to the normalized background fluorescence intensity (F), i.e., the fractional change in fluorescence intensity ($\Delta F/F$), was calculated at each pixel in each frame. If F was less than 0.25, then $\Delta F/F$ was set to be zero [19, 20]. A negative $\Delta F/F$ corresponds to membrane depolarization [21].

We characterized optically recorded action potentials by three parameters: action potential duration at 50% repolarization level (APD50), the slope of upstroke (phase-0 slope), and the slope of the pacemaker depolarization (phase-4 slope). For the estimation of action potential characteristics, we applied spatial filtering, i.e., optical signals of each pixel were replaced with averages of signals of neighbor 5 × 5 pixels. The method to estimate these parameters was as follows: APD50 was calculated as the interval between the 50% depolarization point on the upstroke and the 50% repolarization point on the downstroke of the action potential. Then, the slope of upstroke (phase-0 slope) was estimated by a least-squares fit of a straight line (line 1 in Fig. 1) to a neighborhood region of the 50% depolarization point on the upstroke. By extending the straight line leftward and finding the intercept with the x-axis (time-axis) set at the maximum diastolic potential (MDP) level, a tentative onset of phase-0 was determined. A least-squares fit of the second straight line (line 2 in Fig. 1) to the region from the tentative onset of phase-0 to the point 100 frames before was calculated as the phase-4 slope. As depicted in Fig. 1, the phase-4 diastolic depolarization of SAN cells consists of an almost linearly rising slow subphase (early phase-4) followed by an exponentially rising rapid subphase (late phase-4) [1, 22]. The parameter we evaluated as the phase-4 slope is the slope of the early phase-4. The onset of phase-0 slope was defined as the intersection between line 1 and line 2. These action potential characteristics were calculated for each pixel. To further eliminate artifacts associated with cell contraction,

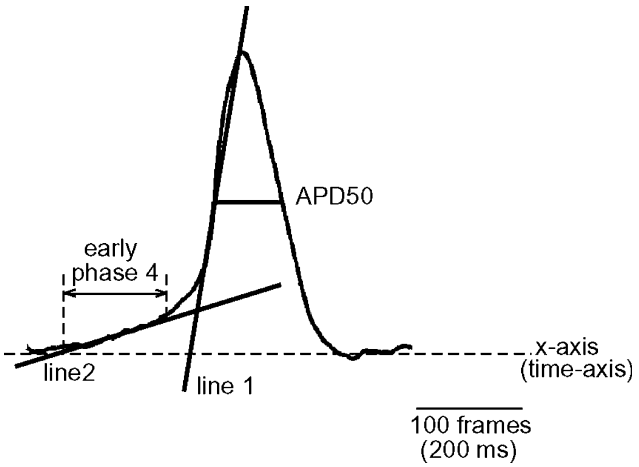

Fig. 1 Action potential in each pixel is characterized by three parameters: phase-0 slope, early phase-4 slope and APD50. *Lines 1* and *2* are least-squares fits of a straight line, representing phase-0 and phase-4 slopes, respectively. The *horizontal dotted line* indicates the x-axis (time-axis). Frame rate was 2.0 ms in most cases, so that 100 frames corresponded to 200 ms

we set appropriate thresholds for these parameter values. When calculated values were out of the range defined by these thresholds, the data were eliminated. Activation maps were drawn by an imaging data analysis software (BV Analyzer, BrainVision, Tokyo, Japan) based on the area where $-\Delta F/F$ exceeds a user-defined threshold. We compared locations of the leading pacemaker site judged from BV Analyzer-produced activation maps and those judged from pseudocolor maps of phase-0 onset, and confirmed that they were equivalent in all cases.

Microelectrode recording

The transmembrane action potential of SAN myocytes was recorded intracellularly with a glass microelectrode (20–50 MΩ) filled with 3 M KCl [15–17]. The output of the microelectrode amplifier (MEZ-7200, Nihon Kohden, Tokyo, Japan) was fed into the optical recording system.

Model simulation

We developed a two-dimensional sheet model, which consisted of 25 × 25 Kyoto-model SAN cells [23]. Each cell was randomly assigned the L-type Ca^{2+} current amplitude within a range of 0.5 to 1.5 times the control to simulate inhomogeneous structure of the SAN. This resulted in a random distribution of intrinsic cycle lengths of SAN pacemaker cells ranging from 247 to 361 ms. The L-type Ca^{2+} current amplitude was reduced for cells on the edges as a boundary condition in order to avoid a corner of the sheet being the leading pacemaker. Other model parameter values (e.g., cell size and ion channel

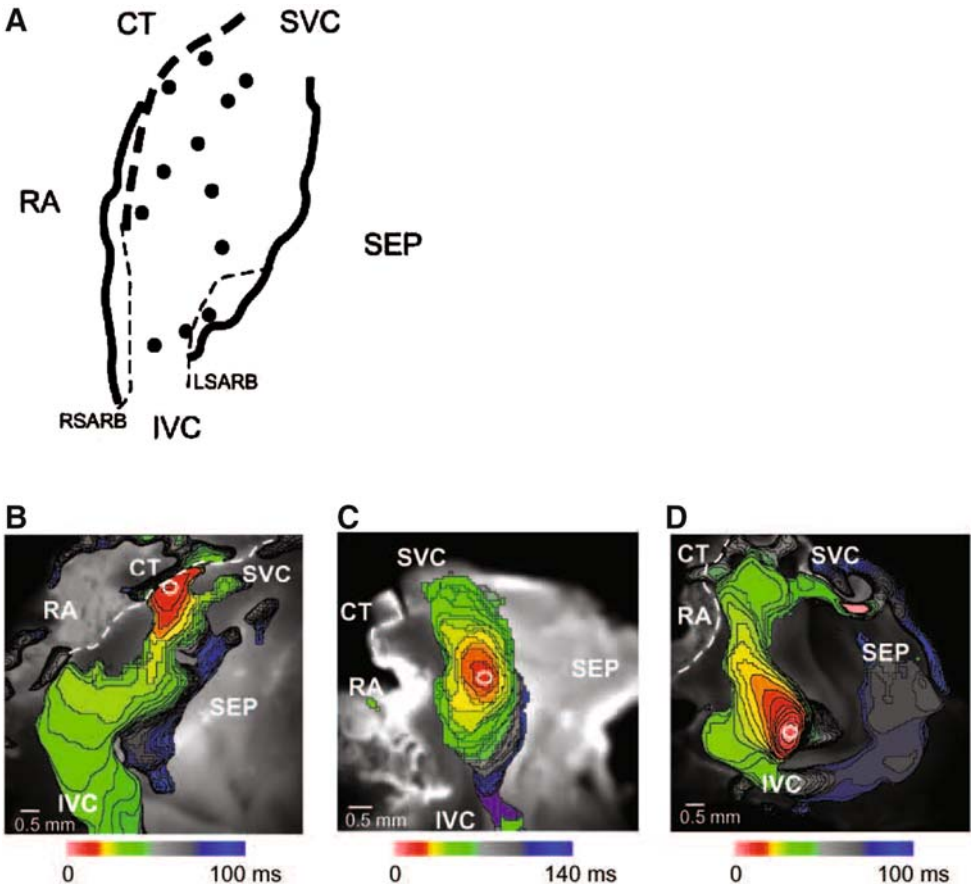

Fig. 2 The locations of the leading pacemaker and the patterns of excitation propagation were diverse among preparations but consistent in each SAN preparation. **a** Schematic diagram of leading pacemaker sites in the SAN. Leading pacemaker sites in 12 different experiments are indicated by *dots*. **b–d** Activation maps of pacemaker activity. Excitation propagation initiated near the SVC (**b**), center (**c**), and IVC (**d**) of the SAN. Isochrones were calculated at 2-ms intervals from the leading pacemaker site. *IVC* Inferior vena cava, *SVC* superior vena cava, *SEP* internal septum, *RA* right atrium, *CT* crista terminalis, *RSARB* right sinoatrial ring bundle, *LSARB* left sinoatrial ring bundle

conductance) were the same as described in the original article [23]. Each cell was electrically coupled with neighboring cells via gap junctions. The intercellular coupling conductance was assigned a constant value or randomly assigned within a given maximum gap junction conductance. The numerical integration algorithm described by Michaels et al. [24] was used for calculating the current through gap junctions, where the current from one cell to its neighbor was derived from Ohm's law as the difference in their membrane potential multiplied by the gap junction conductance, and the total gap junction current I_{couple} was formulated as the sum of currents through gap junctions with neighboring cells (J):

$$I_{\text{couple}} = \sum_{j \in J} g^{j}_{\text{couple}}(V - V_j)$$

where g^{j}_{couple} is the gap junction conductance with a neighboring cell j and V_j is the membrane potential of cell j. I_{couple} was assumed to be carried by K^+ ions, and was incorporated into the total K^+ current for the calculation of $\frac{d[K^+]_i}{dt}$.

Simulations were repeated using an alternative single cell model described by Zhang et al. [25] (Zhang-model cell) and a larger (100 × 100 cells) model scale.

Statistical analysis

All values are presented as mean ± SEM. Statistical significance was determined by repeated-measures analysis of variance (ANOVA). A P-value less than 0.05 was considered significant.

Results

Excitation propagation mapped by voltage imaging

Although it has been reported that di-4-ANNEPPS increases cycle length and its variability at 37°C, the cycle length variability could be reduced when the preparation was kept at 34.0°C [10]. The mean heart rate of isolated SAN tissues at this temperature was 125.3 ± 6.5 beats/min, which fell within a reasonable range as compared to the previously reported values [10, 26].

In all preparations, we successfully recorded optical signals associated with the propagation of pacemaker activity on the endocardial surface of the SAN. Excitation initiated at the same site and propagated through the same conduction pathway in each consecutive optical measurement. The conduction velocity from the leading pacemaker

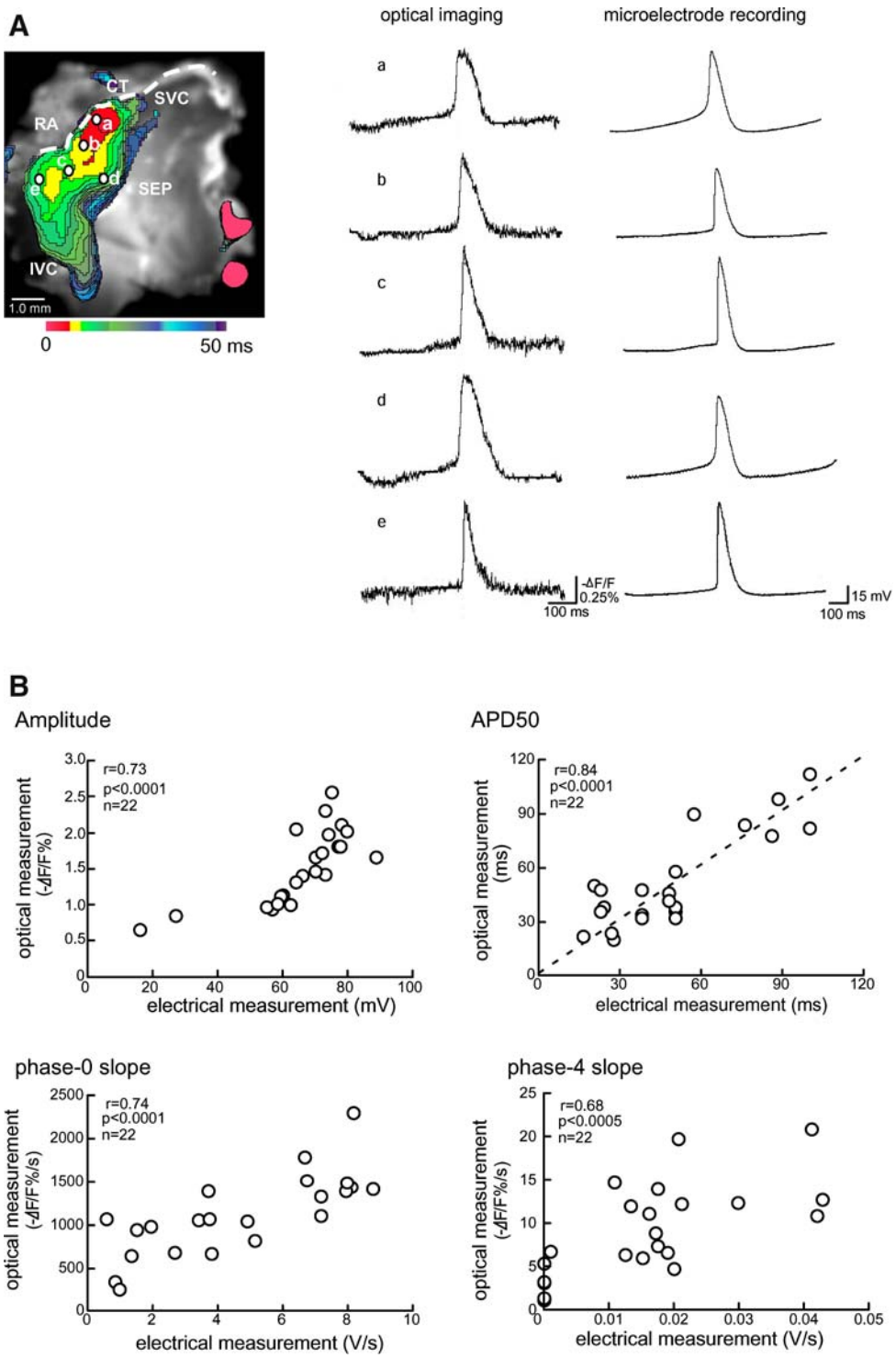

Fig. 3 The estimation of action potential characteristics from optical signals is feasible. **a** Comparison of signal trajectories between optical recordings and microelectrode recordings. The *left panel* shows a representative activation map of the SAN, on which simultaneous optical and microelectrode recordings were performed. Action potentials recorded intracellularly and optically at positions *a–e* are shown in the *right panel*. Isochrones were calculated at 2-ms intervals from the leading pacemaker site. The crista terminalis is delineated by the *dashed line*. *IVC* Inferior vena cava, *SVC* superior vena cava, *SEP* internal septum, *RA* right atrium, *CT* crista terminalis. **b** Correlation between parameter values of electrically and optically recorded action potentials. The *dotted line* in the APD50 panels is the line of identity

site differed depending on the direction of excitation propagation, and thus we measured the fastest conduction velocity as the representative value. The average conduction velocity in all preparations was 5.64 ± 0.79 cm/s. The leading pacemaker site was located at anatomically different points in each SAN preparation ($n = 12$, Fig. 2a). In 5 out of 12 cases, the leading pacemaker site was located at the center region of the SAN. However, in the other 7 preparations, the leading pacemaker site was close to the SVC or the IVC.

The excitation propagation spread along a specific conduction pathway from the leading pacemaker site. There were three propagation patterns. When the leading pacemaker site was located close to the SVC, the excitation

propagated toward the IVC along the CT or the internal septum (Fig. 2b). When the leading pacemaker site was at the center region, the excitation spread bidirectionally toward the SVC and the IVC, and then to the posterior direction toward the atrioventricular node (Fig. 2c). When the leading pacemaker site was close to the IVC, the excitation propagated toward the atrioventricular node and further spread to the SVC (Fig. 2d). Excitation did not propagate to the septum in any preparation.

Validity of estimating action potential characteristics by optical signals

Contraction of SAN cells can produce motion artifacts and distort fluorescent depolarization signals in optical recording experiments, although the artifacts mainly influence the repolarization phase of action potentials [12]. To test the validity of estimating action potential characteristics from optical signals, we compared optically recorded action potential shapes with those electrically recorded with microelectrodes at the same recording sites. Electrically recorded action potential shapes matched well with those of optically recorded action potentials at each corresponding location (Fig. 3a). It is noteworthy that the phase-4 slope did not change in a gradient manner from the leading pacemaker site to the periphery in either optical or intracellular recordings. This was consistent with our preliminary intracellular recording studies ($n = 15$), in which we observed different degrees of diastolic depolarization even within the compact region of the SAN. Moreover, in the preliminary studies, approximately 20% of SAN cells, recorded randomly from the whole area of isolated SAN preparations, showed spontaneous activity without phase-4 depolarization (driven action potential), although we did not systematically map the recording sites depending on whether the recording site is central or peripheral. We then evaluated correlations between action potential parameter values estimated from optical signals and those calculated from intracellularly recorded electrical potentials at the same recording sites. Correlation coefficients in a representative preparation were as follows (Fig. 3b): amplitude ($r = 0.73$, $P < 0.0001$), APD50 ($r = 0.84$, $P < 0.0001$), phase-0 slope ($r = 0.74$, $P < 0.0001$), and phase-4 slope ($r = 0.68$, $P < 0.0005$). Similar degrees of correlation (correlation coefficients ranged between 0.73 and 0.9) were obtained in the other two preparations.

Correlation between leading pacemaker site generation and distribution of action potential characteristics

To explore whether the leading pacemaker site has any correlation with the distribution of action potential characteristics, we made pseudocolor maps for the values of action potential parameters, APD50, the phase-0 slope, and the phase-4 slope. In addition, we showed optical membrane potential trajectories of the region of the leading pacemaker site (open circles) and the region of maximum phase-4 slope (open triangles) (Fig. 4). In 3 of 12 preparations, there existed only a single region where phase-4 slope became maximum, and the leading pacemaker site occurred in the region of maximum phase-4 slope (Fig. 4a). In four other preparations, there were multiple regions where the phase-4 slope became locally maximum, and the leading pacemaker site emerged in one of the regions with locally maximum phase-4 slope (Fig. 4b). In five other preparations, there existed only a single region where phase-4 slope became maximum, but it did not coincide with the leading pacemaker site (Fig. 4c). We analyzed in more detail the representative case in Fig. 4c where the leading pacemaker site did not coincide with the region of maximum phase-4 slope (Table 1). As compared to the leading pacemaker site (open circle in Fig. 4c), the region identified as having maximum phase-4 slope in the pseudocolor map (open triangle in Fig. 4c) had consistently and significantly greater phase-4 slope ($P < 0.01$) in repeated optical measurements ($n = 9$). We made repeated-measures ANOVA in the other two cases where the leading pacemaker site did not coincide with the region with maximum phase-4 slope in the pseudocolor map and confirmed that there existed statistically significant differences.

Fig. 4 The leading pacemaker site did not necessarily occur in the region of maximum action potential duration and maximum phase-4 slope. The pseudocolor images represent the activation map and the spatial distributions of the onset of activation, the phase-0 slope, the phase-4 slope, and APD50, respectively. The leading pacemaker site (*open circles*), and the region of maximum phase-4 slope (*open triangles*) if it does not coincide with the leading pacemaker site, are indicated. Isochrones were calculated at 2-ms intervals from the leading pacemaker site. **a** A case in which there exists a single region of globally maximum phase-4 slope and the leading pacemaker site coincided with it. **b** A case in which there exist multiple regions of locally maximum phase-4 slope and the leading pacemaker site occurred in one of these regions. **c** The leading pacemaker did not emerge at the site of maximum phase-4 slope. Note that optical imaging was performed at a relatively high magnification in this case, and thus ΔF/F was higher than that of other cases. **d** Optical membrane potential trajectories of the region of leading pacemaker site (*open circles*) and the region of maximum phase-4 slope (*open triangles*) in **a**–**c**. *IVC* Inferior vena cava, *SVC* superior vena cava, *SEP* internal septum, *RA* right atrium

Role of gap junction in emergence of leading pacemaker site

Carbenoxolone (100 μM) significantly reduced the conduction velocity of excitation from 5.75 ± 0.18 cm/s to 2.48 ± 0.45 cm/s ($n = 6$, $P < 0.05$) without changing the

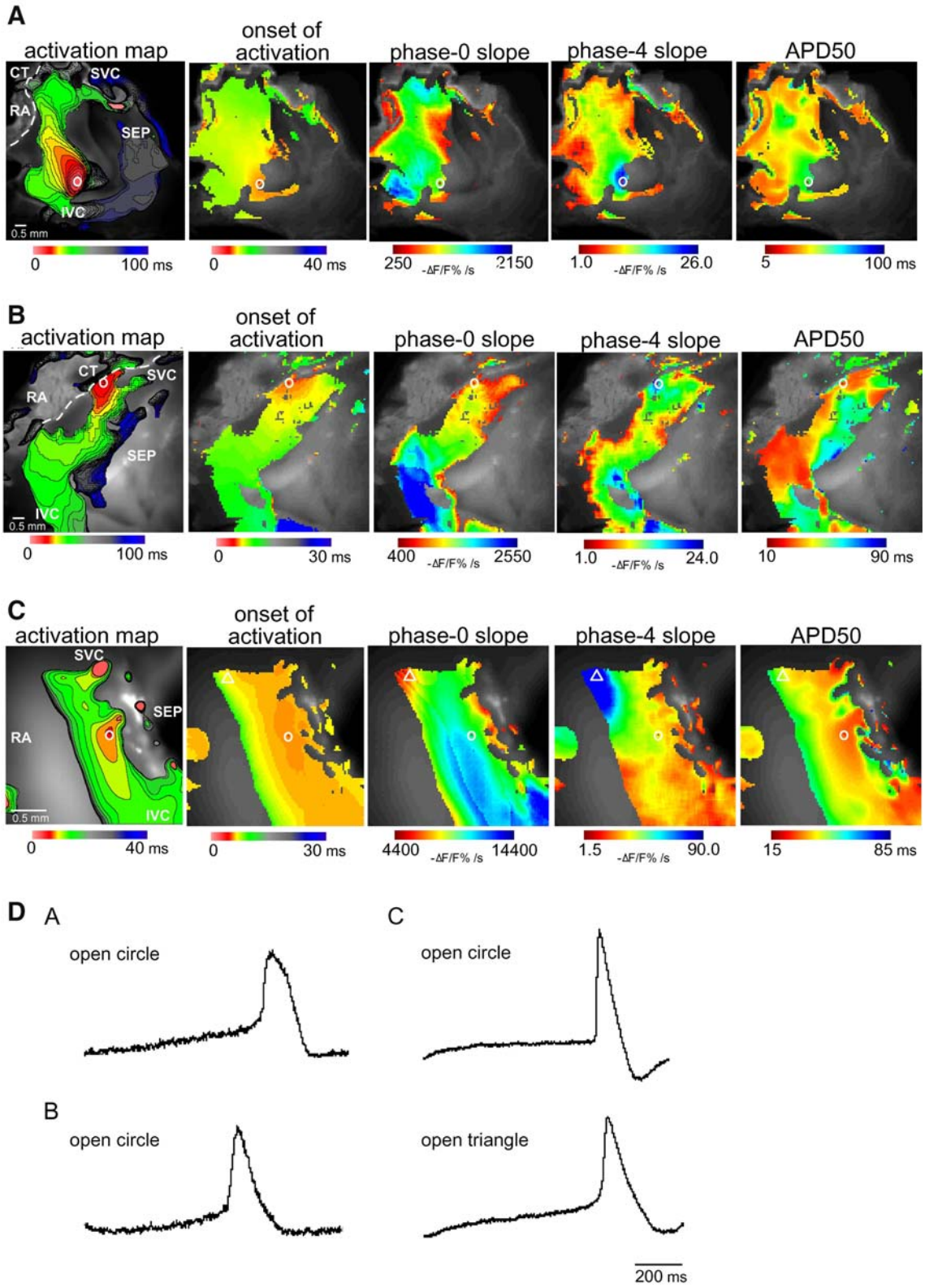

spontaneous beating rate (92.3 ± 4.0% of the control). Pacemaker shifts occurred in all cases ($n = 6$). The new leading pacemaker site emerged at a neighboring location in three cases and at a distant location in three other cases. In the case shown in Fig. 5, the spatial distribution of phase-0 slope was drastically altered by the reduction of electrical

Table 1 The comparison of action potential parameter values between the open circle (the leading pacemaker site) and the open triangle (the region of maximum phase-4 slope) in Fig. 4c ($n = 9$)

	Slopes ($-\Delta F/F$%/s)		APD50 (ms)
	Phase 0	Phase 4	
Open circle	9641 ± 131	19.0 ± 1.9	44.7 ± 0.5
Open triangle	5381 ± 103*	85.5 ± 4.9*	75.6 ± 0.4*

Values are means ± SEM in 9 consecutive recordings

* $P < 0.01$

coupling, but changes in spatial distributions of phase-4 slope and APD50 were moderate. This is probably because the pacemaker shift preferentially affected the phase-0. We also observed different degrees of changes in spatial distributions of phase-0 slope, phase-4 slope, and APD50 in the other two cases after the application of carbenoxolone.

Model simulation

Model simulation resulted in a stable pattern of 1:1 entrainment of all SAN cells with an appropriate value of gap junction conductance. The activation pattern showed action potential conduction spreading radially from the leading pacemaker site. In the representative case 1 (Fig. 6a), the global cycle length was 290 ms at the gap junction conductance of 20 nS/cell and 286 ms at 10 nS/cell. The cell with the shortest intrinsic cycle length was in the upper middle region (asterisk in Fig. 6a). With 20-nS gap junction conductance, the leading pacemaker site appeared at the lower middle region, however, the cell with the maximum early phase-4 slope was located at the left lower corner. To analyze the cause of the dissociation between the leading pacemaker site and the cell with the maximum early phase-4, we compared the simulated action potential trajectories of the two locations. As shown in Fig. 6a (inset), the leading pacemaker site had a steeper exponentially rising late phase-4 slope as compared to the cell with the maximum early phase-4 slope. When the maximum gap junction conductance was lowered to 10 nS, the leading pacemaker site shifted to the left lower corner. The reduction in gap junction conductance influenced the distribution of phase-4 slope values of SAN cells, and the leading pacemaker site shifted to the region of maximum phase-4 slope but did not coincide with the region of maximum APD50. In the representative case 2 (Fig. 6b), the leading pacemaker site and the region of maximum phase-4 slope were at the left upper region with 20-nS gap junction conductance, although they did not completely match. The reduction in gap junction conductance to 10 nS induced a shift of the leading pacemaker site to the regions of locally maximum phase-4 slope. In both cases, MDP map matched phase-4 slope map, indicating that cells with greater phase-4 slope have more depolarized MDPs.

We repeated simulations ($n = 10$ in total) and obtained similar results in all trials. Namely, the leading pacemaker site did not necessarily coincide with the region of maximum early phase-4 slope with 20 nS gap junction conductance, and the reduction in gap junction conduction often shifted the leading pacemaker site to the regions of locally maximum phase-4 slope. Additionally, we tested the robustness of our model by increasing the number of cells to 50×50 ($n = 3$). Also, we randomly changed the gating property for the L-type Ca^{2+} current–voltage dependency where gating shifts ranged from -5 to $+5$ mV ($n = 10$), which resulted in a random distribution of intrinsic cycle length of SAN pacemaker cells ranging from 268 to 371 ms. These variations yielded the same results. A random assignment of the gap junction conductance did not change the result of simulations significantly. The relationship between the leading pacemaker site and the site of maximum early phase-4 slope, and the shift of the leading pacemaker site to a distant locally maximum phase-4 slope region by reducing the gap junction conductance in the model simulation well agreed with our experimental observations. We further conducted a simulation study assuming a model with a gradient distribution of amplitudes of L-type Ca^{2+} currents from the center to the periphery, but the model did not reproduce the dissociation between the leading pacemaker site and the region of maximum early phase-4 slope.

To test whether the results of simulations depend on the choice of a single-cell model, we repeated simulations using 100×100 Zhang-model cells ($n = 6$). Since changes in either L-type Ca^{2+} current density or "funny" pacemaker current (I_f) density did not significantly alter the inherent cycle length of a Zhang-model cell, we randomly assigned T-type Ca^{2+} current density within a range from 0 to 200% of the original value given for the central region. Increases in a model scale to 100×100 resulted in more complex dynamics of pacemaker synchronization. We observed multiple regions where phase-4 slope became locally maximum, and the leading pacemaker site emerged in one of the regions with locally maximum phase-4 slope (Fig. 7a). We also observed cases ($n = 2$) where the leading pacemaker site dissociated from the region of (locally) maximum phase-4 slope (Fig. 7b). The dissociation was partly explained by the differences in MDP and the slope of the exponentially rising late phase-4. Namely, in such cases, the leading pacemaker site either had a more depolarized MDP (as shown in Fig. 7b inset) or a steeper late phase-4 slope as compared to the regions of locally maximum phase-4 slope. These simulations suggest that,

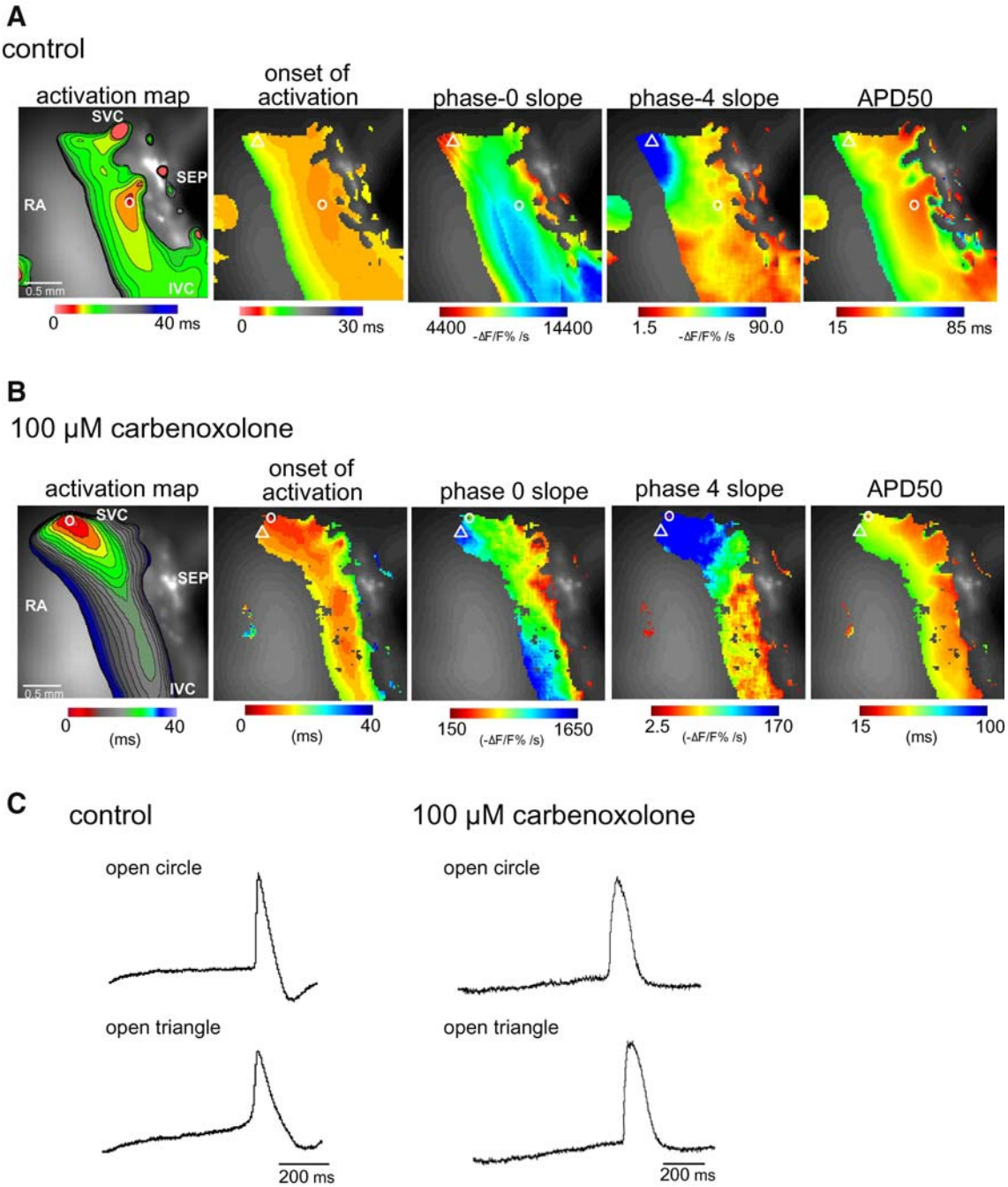

Fig. 5 Carbenoxolone changed the spatial distribution of optical action potential parameter values and induced pacemaker shifts. Representative pseudocolor images of the control (**a**) and those after the application of carbenoxolone (**b**) are shown. The *open circles* and *open triangles* indicate the leading pacemaker site and the site of maximum phase-4 slope, respectively. **c** Optical membrane potential trajectories of the region of leading pacemaker site (*open circles*) and the region of maximum phase-4 slope (*open triangles*) in **a** and **b**. *SVC* Superior vena cava, *SEP* internal septum, *RA* right atrium

irrespective of the model scale and the choice of a single-cell model, there exist multiple regions where phase-4 slope becomes locally maximum, and the leading pacemaker site does not necessarily coincide with the region of maximum early phase-4 slope.

Discussion

In the present study, we analyzed action potential characteristics in the rabbit SAN by voltage imaging and demonstrated that the leading pacemaker site does not

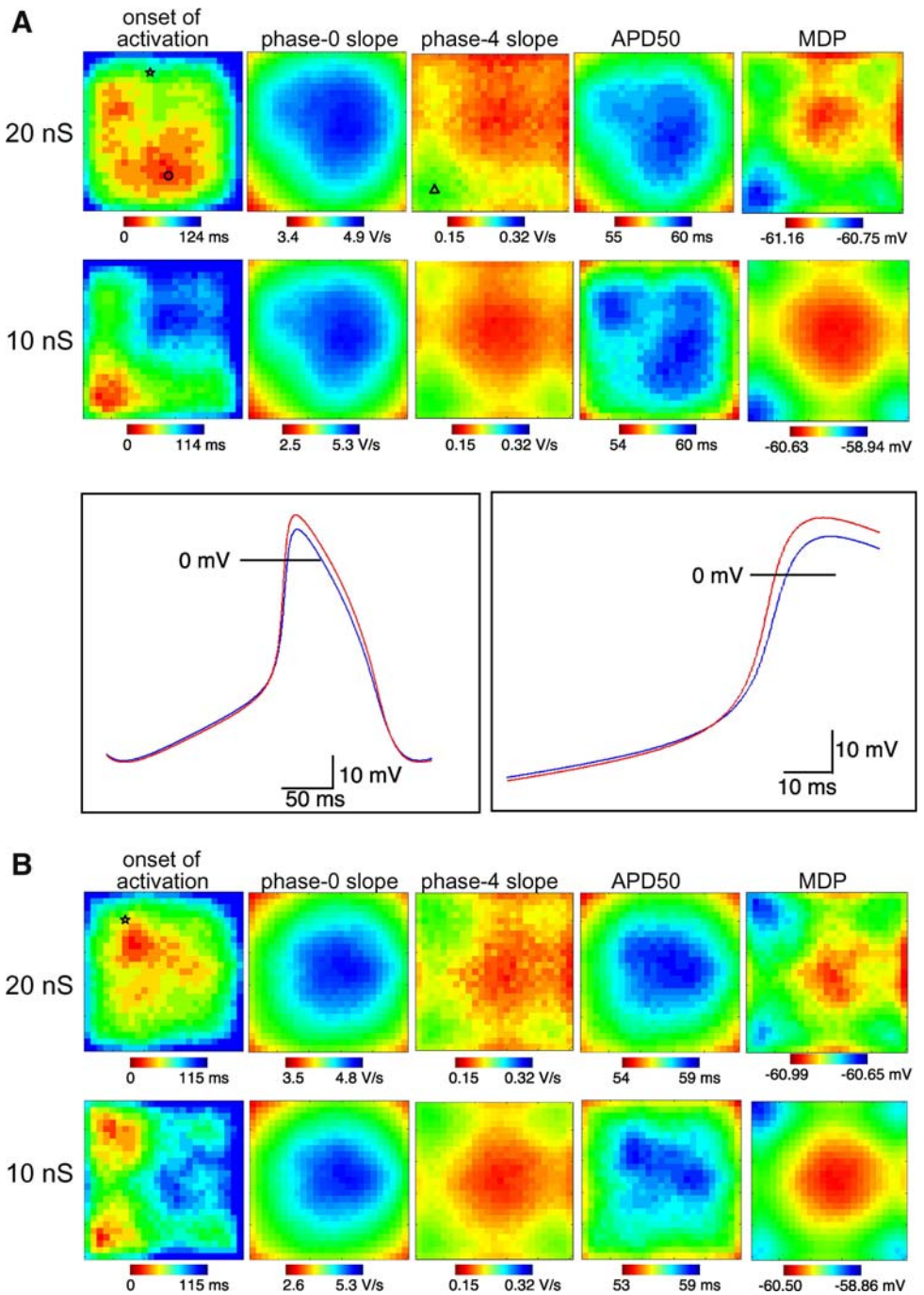

Fig. 6 Model simulation, assuming an inhomogeneous distribution of intrinsic properties of SAN cells, reproduced dissociation between the leading pacemaker site and the region of maximum phase-4 slope. A two-dimensional sheet model consisting of 25 × 25 Kyoto-model SAN cells was evaluated. Random distributions of L-type Ca^{2+} current amplitudes were assumed to simulate the inhomogeneous structure of the SAN. *Upper* and *lower panels* represent the activation patterns with gap junction conductances of 20 and 10 nS/cell, respectively. The *asterisk* indicates the location of the cell that has the shortest cycle length. **a** The dissociation between the leading pacemaker site and the cell (site) with the maximum linearly rising early phase-4 with the gap junction conductance of 20 nS/cell is explained by a steeper exponentially rising late phase-4 slope at the leading pacemaker site shown in the *inset*. The *left panel* indicates entire action potential waveforms and the *right panel* shows expanded action potential waveforms. The *red trace* illusrates the action potential trajectory of the leading pacemaker site (*open circle on activation map*); the *blue trace* presents the action potential trajectory of the cell with the maximum phase-4 slope (*open triangle on phase-4 slope map*). The reduction in the gap junction conductance changed the spatial distribution of action potential characteristics and shifted the leading pacemaker site. The leading pacemaker site shifted from the lower center to the bottom left corner where the phase-4 slope was the maximum. **b** The reduction in the gap junction conductance caused bifocal activation in the left region. These new leading pacemaker sites coincided with regions of locally maximum phase-4 slope

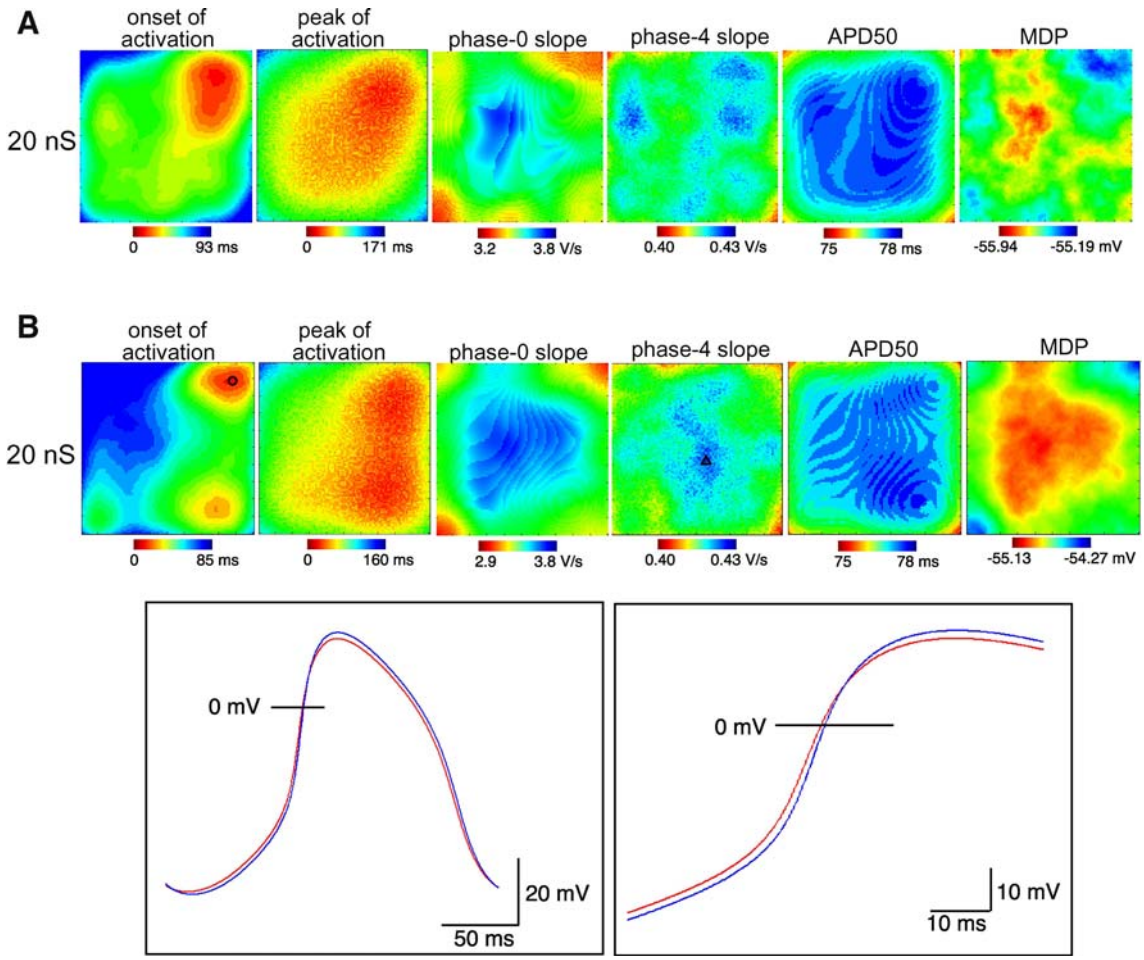

Fig. 7 Two representative simulation results of 100 × 100 Zhang model cells. In **a**, there were multiple regions where phase-4 slope became locally maximum, and the leading pacemaker site emerged in one of the regions with locally maximum phase-4 slope. In **b**, the leading pacemaker site dissociated from the region of maximum phase-4 slope. The dissociation is explained by a more depolarized MDP at the leading pacemaker site shown in the *inset*. The *left panel* indicates entire action potential waveforms and the *right panel* shows expanded action potential waveforms. The *red trace* illustrates the action potential trajectory of the leading pacemaker site (*open circles on activation map*); the *blue trace* illustrates the action potential trajectory of the cell with the maximum phase-4 slope (*open triangle* on phase-4 slope map)

necessarily emerge in the region of maximum action potential duration and maximum early phase-4 slope. These results suggest that the SAN structure is more inhomogeneous than dictated by the gradient model or the mosaic model. It is postulated that the leading pacemaker site is formed as a consequence of mutual interaction of a large number of cells in the compact region of the SAN [24]. Given that distribution of membrane potential properties is more inhomogeneous than a gradient distribution, the reduction in mutual interaction should have a more pronounced effect on the action potential propagation. Our observation that the gap junction blockade induced changes in action potential characteristics and phase shifts agrees with the prediction. Further, our simulation validated the idea that inhomogeneous distribution of membrane properties could induce discrepancy between the leading pacemaker site and the region of maximum early phase-4 slope.

Technical consideration

Optical signals we measured are changes in fluorescence intensity of a single wave band ($\lambda > 590$ nm), which inversely correlate with membrane potentials [21]. In the present study, the fluorescent signal at each trial was evaluated as the change relative to the reference fluorescence intensity; therefore, the absolute membrane potential value, e.g., MDP, cannot be assessed. Although optical techniques using voltage-sensitive dyes are useful to simultaneously analyze electrical activity and propagation mechanisms of the heart at a tissue level, there exist

technical problems such as motion artifact and limitation of spatiotemporal resolution [12]. Nygren et al. showed that the rise time of optical action potential (phase-0) was slower than that recorded with a microelectrode technique in the adult mouse heart [27]. This is because optically recorded action potential represents spatially averaged transmembrane potentials. In the present study, although action potential characteristics estimated from optical signals fairly well correlated with those obtained by intracellular recording, they showed a slight discrepancy. As we mentioned in the "Results" section, in the preliminary studies we observed different degrees of diastolic depolarization within the compact region of the SAN. Apart from the measurement noise, we consider that the discrepancy is partly induced by spatial averaging of multiple SAN cells with heterogeneous action potential characteristics.

As shown in Figs. 3 and 4, the nonlinear time course of phase-4 depolarization, which consists of a linearly depolarizing early phase and a rapidly depolarizing curvilinear late phase, is not clear in optical tracings. Although the response of the dye we used is fast enough to trace the action potential, there is a possibility that $-\Delta F/F$ could not faithfully follow the changes in membrane potential during the late phase due to nonlinear properties of the voltage-sensitive dye.

Further limitation of our optical imaging method is that the voltage-sensitive dye, di-4-ANEPPS, could induce photodynamic damage to cardiomyocytes [28]. The toxic effect of the dye may have caused an increase in cycle length and heart rate variability. As described in the "Methods" section, we minimized the exposure time of excitation light, reduced intensity of excitation light, and lowered the temperature of the preparation to avoid photodynamic damage of the tissue. However, the toxicity of the dye might still have influenced the results slightly.

Leading pacemaker site and excitation propagation in SAN

We observed that propagation patterns of pacemaker activity in the rabbit SAN differ, and the location of the leading pacemaker site is also variable (Figs. 2 and 4). The leading pacemaker site was not necessarily next to the CT. These results agree with previous reports that showed diverse locations of the leading pacemaker site as well as various excitation propagation patterns [10]. Morphological characteristics and these diversities may have correlation. Nerves, ganglia, and myocytes constitute the complex anatomical structure of the SAN [8]. Moreover, immunohistochemical observation suggested that the α actin-positive, neurofilament-positive, and connexin43-negative region between the SVC and IVC might play a role in generating the leading pacemaker site [8, 29]. These complexities of the SAN structure may underlie the leading pacemaker site formation and cause the diversity of its location. Our results, in which the leading pacemaker site appeared at various locations, are compatible with this notion.

The excitation propagation showed various patterns in the present study, however, there were several characteristics common to all preparations. Excitation did not propagate to the septum, and the block zone existed between the SVC and the IVC in the SAN. This transmission blockade could be due to a poor electrical coupling between cells or poor excitability [30]. It has been reported that the preferential conduction from the leading pacemaker site is in the oblique cranial direction or the caudal direction to the CT [1, 31]. Our results are consistent with these reports. The SAN contains abundant myofilaments and collagen fibers although its contents differ among species and ages [7, 8, 32]. These fibers, especially myofilament, may influence the conduction pathway. The collagen content does not affect the conduction velocity [33], but an increase in myofibroblast density decreases the diastolic potential and action potential upstroke [34]. The existence of the conducting pathway may serve to protect against irregular conduction such as reentry and invasion of action potential from outside of the SAN.

Cell-to-cell interaction through gap junctions and interpretation of pacemaker shift

Gap junctions have been believed to contribute to a low resistance intercellular electrical pathway that facilitates the propagation of electrical signals and the synchronization of beating cells in the SAN [35]. Several types of gap junction protein, connexins, are expressed in the rabbit SAN [36]. In the center of the SAN, connexin40, connexin45, and connexin46 are abundantly expressed, but there is virtually no expression of connexin43, and those connexins are thought to contribute to proper excitation propagation in the SAN [29].

The overall effect of gap junction blockade on the SAN function is a decrease in conduction velocity. It is possible that the pacemaker shift is responsible for the change in propagation pathway along different fiber orientations and the subsequent change in conduction velocity. The role of each connexin subtype in the SAN has not been clearly understood, but they may contribute to varying the conduction velocity depending on the direction of excitation propagation [10, 31].

The present study indicates that gap junctions do not merely conduct excitation from the leading pacemaker,

but importantly affect action potential characteristics and determine the leading pacemaker site. We suggest that regional differences in the density and composition of gap junction subtype proteins should be interpreted in this context. For instance, changes in the gap junction density and/or composition associated with aging may shift the leading pacemaker site and lead to an aberrant conduction.

The mechanism of changes in action potential characteristics by slowing conduction velocity could be a "democratic" process of mutually coupled cells [9]. Alternatively, a decrease in conduction velocity may affect intrinsic SAN cell properties by a cellular mechanism. For example, reduction in conduction velocity increases the restitution time of intracellular Ca^{2+} cycling [37]. This could alter intrinsic cellular properties and shift the leading pacemaker site.

Significance of model simulation

Our model assumes that intrinsic cellular properties of SAN cells are randomly distributed, and subsequently, inherent cycle lengths of SAN cells are randomly distributed. However, we by no means claim that the actual structure of the SAN is completely random; instead, we intended to simulate the situation in which the pacemaker organization is more inhomogeneous than a simple gradient configuration due to various anatomical constraint. Of course, such anatomical constraint is much more precisely reconstructed by a sophisticated three-dimensional model [38], however, a two-dimensional sheet model is simpler and sufficient to understand the mechanism underlying the dissociation between the leading pacemaker site and the region of maximum early phase-4 slope.

The current version of our model is simplistic in the sense that it does not include atrial tissue at the boundaries, and thus electrotonic modulations of atrial cells were not taken into account, although the boundary condition (decrease in L-type Ca^{2+} current amplitude) suppresses the excitation of cells on edges. Further, the maximum number of cells we tested was $100 \times 100 = 10{,}000$, which corresponded to only a small fraction of the compact region of the SAN. However, an increase in the model scale should add further complexity to the dynamic behaviors of the model SAN, irrespective of the boundary condition. Therefore, we infer that similar results, i.e., the existence of multiple regions of locally maximum phase-4 slope, and the dissociation between the leading pacemaker site and the region of maximum early phase-4 slope, would be observed in models with larger sizes. Distant cells are less influenced by each other and should tend to behave independently. We predict that if there exists a region with more depolarized MDP or steeper late phase-4 distant from the region of maximum early phase-4, the region could be the leading pacemaker site.

We first focused on the inhomogeneous distribution of L-type Ca^{2+} current properties because the effects of changes in L-type Ca^{2+} current kinetics and amplitudes on the action potential duration and the inherent cycle length of Kyoto-model SAN cell were well documented [23]. A random distribution of gap junction conductance added further complexity to the regional differences in action potential characteristics, but the simulation results were essentially the same. Heterogeneity of other currents such as Na^+ current, delayed-rectifier K^+ current, and hyperpolarization-activated cation current has also been reported previously [6]. We tested the effects of random distribution of T-type Ca^{2+} current amplitudes, which significantly influence the cellular inherent cycle length, on the behavior of the Zhang-model SAN. Again, we observed cases where the leading pacemaker site and the region of maximum early phase-4 slope did not match, although in a majority of cases, the leading pacemaker site occurred in the region of locally maximum phase-4. In the present study, we randomized a single parameter while keeping other parameters constant to dissect the effect of each factor separately. Although we did not thoroughly examine effects of randomization of all ion channels, we predict that randomization of any combination of parameters that influence the inherent cycle length of a model cell will cause similar results. The model reproduced the dissociation between the leading pacemaker site and the region of maximum early phase-4 slope and showed a jump of the leading pacemaker site by the reduction in gap junction conductance as observed in the present imaging experiments. With an increase in model scale, multiple regions of locally maximum phase-4 slope emerged and the leading pacemaker site coincided with one of these locally maximum phase-4 slope regions in a majority of cases. These features of simulation results are parallel with those observed experimentally and may be caused by common underlying mechanisms.

In simulations, the dissociation was caused by multiple factors. One factor was the slope of the late phase-4, an exponentially rising subphase of phase-4, which partly depends on L-type Ca^{2+} current amplitude. When the region of maximum early phase-4 slope had a relatively small L-type Ca^{2+} current amplitude and subsequently a relatively gentle late phase-4 slope, a region with higher L-type Ca^{2+} current amplitude and subsequently a relatively steep late phase-4 slope became the leading pacemaker site (as in the case of Fig. 6a). Another factor is the differences in MDP. There were cases in which the region with a more depolarized MDP reached the threshold to initiate an action potential earlier than the region of maximum early phase-4 slope and became the leading

pacemaker (as in the case of Fig. 7b). We therefore suggest that regional differences in cellular properties are more complex than a simple gradient structure. This by no means denies the existence of a gradient structure. Gradient distributions of averaged electrical properties and mean parameter values should be present, even though electrical properties of individual cells are diverse.

In summary, estimation of action potential characteristics from optical signals was feasible. There were cases where multiple regions of locally maximum phase-4 slope existed, and the leading pacemaker site occurred in one of these regions. Further, there were cases where the leading pacemaker site did not coincide with the region of maximum early phase-4 slope. We conclude that the functional structure of the SAN is more inhomogeneous than dictated by previous models. In addition, we suggest that gap junctions not only transmit excitation, but also significantly contribute to the determination of the leading pacemaker site and the action potential characteristics in the SAN.

Acknowledgments We thank S. Kojima and M. Ito-Shiga for technical assistance and R. Ueno and U. Kuze for secretarial work. We also thank Prof. L. Pott of the Department of Physiology Ruhr-University Bochum for his critical reading and advice. This work was supported by a medical research grant from Chiyoda Mutual Life Foundation, Japan, a research grant from the Ministry of Education, Culture, Sports, Science and Technology of Japan (19790546), and Grant-in-Aid for Researchers, Hyogo College of Medicine, 2006.

References

1. Bleeker WK, Mackaay AJ, Masson-Pévet M, Bouman LN, Becker AE (1980) Functional and morphological organization of the rabbit sinus node. Circ Res 46:11–22
2. Boyett MR, Honjo H, Kodama I (2000) The sinoatrial node, a heterogeneous pacemaker structure. Cardiovasc Res 47:658–687
3. Masson-Pévet MA, Bleeker WK, Besselsen E, Treytel BW, Jongsma HJ, Bouman LN (1984) Pacemaker cell types in the rabbit sinus node: a correlative ultrastructural and electrophysiological study. J Mol Cell Cardiol 16:53–63
4. Zhang H, Holden AV, Boyett MR (2001) Gradient model versus mosaic model of the sinoatrial node. Circulation 103:584–588
5. Verheijck EE, Wessels A, van Ginneken AC, Bourier J, Markman MW, Vermeulen JL, de Bakker JM, Lamers WH, Opthof T, Bouman LN (1998) Distribution of atrial and nodal cells within the rabbit sinoatrial node. Circulation 97:1623–1631
6. Kodama I, Nikmaram MR, Boyett MR, Suzuki R, Honjo H, Owen JM (1997) Regional differences in the role of the Ca^{2+} and Na^{2+} currents in pacemaker activity in the sinoatrial node. Am J Physiol 272:H2793–H2806
7. James TN, Kawamura K, Meijler FL, Yamamoto S, Terasaki F, Hayashi T (1995) Anatomy of the sinus node, AV node, and His bundle of the heart of the sperm whale (Physeter macrocephalus), with a note on the absence of an os cordis. Anat Rec 242:355–373
8. Roberts LA, Slocum GR, Riley DA (1989) Morphological study of the innervation pattern of the rabbit sinoatrial node. Am J Anat 185:74–88
9. Jalife J (1984) Mutual entrainment and electrical coupling as mechanisms for synchronous firing of rabbit sino-atrial pacemaker cells. J Physiol 356:221–243
10. Fedorov VV, Hucker WJ, Dobrzynski H, Rosenshtraukh LV, Efimov IR (2006) Postganglionic nerve stimulation induces temporal inhibition of excitability in rabbit sinoatrial node. Am J Physiol Heart Circ Physiol 291:H612–H623
11. Bromberg BI, Hand DE, Schuessler RB, Boineau JP (1995) Primary negativity does not predict dominant pacemaker location: implications for sinoatrial conduction. Am J Physiol Heart Circ Physiol 269:H877–H887
12. Efimov IR, Nikolski VP, Salama G (2004) Optical imaging of the heart. Circ Res 94:21–33
13. Kettlewell S, Walker NL, Cobbe SM, Burton FL, Smith GL (2004) The electrophysiological and mechanical effects of 2, 3-butane-dione monoxime and cytochalasin-D in the Langendorff perfused rabbit heart. Exp Physiol 89:163–172
14. Physiological Society of Japan (1994) Guiding principles for the care and use of animals in the field of physiological sciences. Jpn J Physiol 44:5
15. Masumiya H, Tanaka H, Shigenobu K (1997) Effects of Ca^{2+} antagonists on sinus node: prolongation of late phase 4 depolarization by efonidipine. Eur J Phrmacol 335:15–21
16. Masumiya H, Saitoh T, Tanaka Y, Horie S, Aimi N, Takayama H, Tanaka H, Shigenobu K (1999) Effects of hirsutine and dihydrocorynantheine on the action potentials of sino-atrial node, atrium and ventricle. Life Sci 65:2333–2341
17. Ono K, Masumiya H, Sakamoto A, Christé G, Shijuku T, Tanaka H, Shigenobu K, Ozaki Y (2001) Electrophysiological analysis of the negative chronotropic effect of endothelin-1 in rabbit sinoatrial node cells. J Physiol 537:467–488
18. Kodama I, Boyett MR (1985) Regional differences in the electrical activity of the rabbit sinus node. Pflügers Arch 404:214–226
19. Okada Y, Masumiya H, Tamura Y, Oku Y (2007) Respiratory and metabolic acidosis differentially affect the respiratory neuronal network in the ventral medulla of neonatal rats. Eur J Neurosci 26:2834–2843
20. Oku Y, Masumiya H, Okada Y (2007) Postnatal developmental changes in activation profiles of the respiratory neuronal network in the rat ventral medulla. J Physiol 585:171–186
21. Koura T, Hara M, Takeuchi S, Ota K, Okada Y, Miyoshi S, Watanabe A, Shiraiwa K, Mitamura H, Kodama I, Ogawa S (2002) Anisotropic conduction properties in canine atria analyzed by high-resolution optical mapping: preferential direction of conduction block changes from longitudinal to transverse with increasing age. Circulation 105:2092–2098
22. Bogdanov KY, Maltsev VA, Vinogradova TM, Lyashkov AE, Spurgeon HA, Stern MD, Lakatta EG (2006) Membrane potential fluctuations resulting from submembrane Ca^{2+} release in rabbit sinoatrial nodal cells impart an exponential phase to the late diastolic depolarization that controls their chronotropic state. Circ Res 99:979–987
23. Sarai N, Matsuoka S, Kuratomi S, Ono K, Noma A (2003) Role of individual ionic current systems in the SA node hypothesized by a model study. Jpn J Physiol 53:125–134
24. Michaels DC, Matyas EP, Jalife J (1987) Mechanisms of sinoatrial pacemaker synchronization: a new hypothesis. Circ Res 61:704–714
25. Zhang H, Holden AV, Kodama I, Honjo H, Lei M, Varghese T, Boyett MR (2000) Mathematical models of action potentials in the periphery and center of the rabbit sinoatrial node. Am J Physiol Heart Circ Physiol 279:H397–H421
26. Hof TO, Mackaay AJ, Bleeker WK, Houtkooper JM, Abels R, Bouman LN (1980) Dependence of the chronotropic effects of

calcium, magnesium and sodium on temperature and cycle length in isolated rabbit atria. J Pharmacol Exp Ther 212:183–189
27. Nygren A, Clark RB, Belke DD, Kondo C, Giles WR, Witkowski FX (2000) Voltage-sensitive dye mapping of activation and conduction in adult mouse hearts. Ann Biomed Eng 28:958–967
28. Schaffer P, Ahammer H, Muller W, Koidl B, Windisch H (1994) Di-4-ANEPPS causes photodynamic damage to isolated cardiomyocytes. Pflüger Arch 426:548–551
29. Coppen SR, Kodama I, Boyett MR, Dobrzynski H, Takaghishi Y, Honjo H, Yeh HI, Severs NJ (1999) Connexin45, a major connexin of the rabbit sinoatrial node, is co-expressed with connexin43 in a restricted zone at the noda-crista terminalis border. J Histochem Cytochem 47:907–918
30. Op't Hof T, Bleeker WK, Masson-Pévet M, Jongsma HJ, Bouman LN (1983) Little-excitable transitional cells in the rabbit sinoatrial node: a statistical, morphological and electrophysiological study. Experientia 39:1099–1101
31. Sano T, Yamagishi S (1965) Spread of excitation from the sinus node. Circ Res 16:423–430
32. Camelliti P, Green CR, LeGrice I, Kohl P (2004) Fibrobloast network in rabbit sinoatrial node. Circ Res 94:828–835
33. Opthof T, de Jonge B, Jongsma HJ, Bouman LN (1987) Functional morphology of the mammalian sinuatrial node. Eur Heart J 8:1249–1259
34. Miragoli M, Gaudesius G, Rohr S (2006) Electrotonic modulation of cardiac impulse conduction by myofibroblasts. Circ Res 98:801–810
35. Kanno S, Saffitz JE (2001) The role of myocardial gap junctions in electrical conduction and arrhythmogenesis. Cardiovasc Pathol 10:169–177
36. Verheule S, van Kempen MJ, Postma S, Rook MB, Jongsma HJ (2001) Gap junctions in the rabbit sinoatrial node. Am J Physiol Heart Circ Physiol 280:H2103–H2115
37. Maltsev VA, Vinogradova TM, Lakatta EG (2006) The emergence of a general theory of the initiation and strength of the heartbeat. J Pharmacol Sci 100:338–369
38. Dobrzynski H, Li J, Tellez J, Greener ID, Nikolski VP, Wright SE, Parson SH, Jones SA, Lancaster MK, Yamamoto M, Honjo H, Takagishi Y, Kodama I, Efimov IR, Billeter R, Boyett MR (2005) Computer three-dimensional reconstruction of the sinoatrial node. Circulation 111:846–854